Journal of Fluorine Chemistry 168 (2014) 204–211

Contents lists available at ScienceDirect

Journal of Fluorine Chemistry

journal homepage: www.elsevier.com/locate/fluor

Phase transitions in fluoride KFe_2F_6 with tetragonal tungsten bronze structure

M.V. Gorev [a,b], I.N. Flerov [a,b,*], A. Tressaud [c], M.S. Molokeev [a], A.V. Kartashev [a], E.I. Pogoreltsev [a,b], O.A. Bayukov [a]

[a] L.V. Kirensky Institute of Physics, Siberian Department of RAS, 660036 Krasnoyarsk, Russia
[b] Siberian Federal University, 660074 Krasnoyarsk, Russia
[c] Institut de Chimie de la Matière Condensee, CNRS, 33608 Pessac Cedex, France

ARTICLE INFO

Article history:
Received 26 June 2014
Received in revised form 26 September 2014
Accepted 29 September 2014
Available online 18 October 2014

Keywords:
Tetragonal tungsten bronze structure
Phase transition
Charge ordering
Thermal properties

ABSTRACT

Heat capacity, thermal dilatation, structure, Mössbauer spectra and dielectric permittivity of fluoride KFe_2F_6 with tetragonal tungsten bronze crystal structure were studied. The as-made sample undergoes two structural phase transitions $P4/mbm$ ($T_1 \approx 340$ K) → $Pbam$ ($T_2 \approx 250$ K) → G_2 and magnetic phase transformation at $T_m \approx 133$ K. Heating up to 600–700 K and subsequent cooling in helium atmosphere leads to a change of phase transition temperatures and diffused anomalies in thermal expansion. The results obtained and influence of thermal prehistory of the sample on its physical properties are discussed in the context of previous studies on related fluorides KFe_2F_6, which sometimes suggest conflicting structural details.

1. Introduction

Transition metal fluorides adopting the tetragonal tungsten bronze (TTB) structure with general formula $K_{6-x}M^{2+}{}_{6-x}M^{3+}{}_{4+x}F_{30}$ (M = transition metal, $0 \leq x \leq 2$) have been studied in the past as potential multiferroic materials. $K_{6-x}Fe_{10}F_{30}$ represents probably the most studied fluoride-based material to date, and is interesting for a number of reasons. It has been demonstrated experimentally that members of this series are multiferroic at low temperatures and the exact interplay between ferroelectric, ferroelastic and magnetic ordering parameters is finely tuned by changes in compositions [1–4].

Crystal structure of $K_{6-x}Fe^{2+}{}_{6-x}Fe^{3+}{}_{4+x}F_{30}$ and its dependence on the concentration and temperature was studied intensively and rather contradictory results were obtained. Early work [5] showed that a phase of composition $K_6Fe_{10}F_{30}$ (alternatively formulated as $K_{0.6}Fe^{2+}{}_{0.6}Fe^{3+}{}_{0.4}F_3$) crystallized in TTB structure type, with a polar orthorhombic distortion (space group $Pba2$, $c \approx 2c_{TTB}$) of the Aristotype tetragonal phase (space group $P4/mbm$) at room temperature. Bond distances around the three distinct Fe sites suggested a partial ordering of Fe^{2+}/Fe^{3+}. The small polar deviation from the parent symmetry also suggested the possibility of both ferroelectric and ferroelastic behavior that was later confirmed experimentally [2]. There was proposed a simultaneous, coupled ferroelectric/ferroelastic transition at 490 K, on the basis of dielectric, calorimetric, resistivity and optical measurements, and suggested that Fe^{2+}/Fe^{3+} disordering might be concomitant, with a change of point group from $mm2$ to $4/mmm$. The charge-disordering was later confirmed by Mössbauer spectroscopy [6]. A follow-up investigation of the off-stoichiometric variants $K_{6-x}Fe_{10}F_{30}$ ($0 < x < 0.40$) revealed a remarkable sensitivity of both crystallographic symmetry and ferroelectric properties versus composition. T_C reduces to 230 K for $x = 0.40$ compared to $T_C = 490$ K for $x = 0$ [7].

A later study by Ishihara et al. [8], identified two further phase transitions, one around 120 K being of magnetic origin, and one around 290 K being a structural phase transition observed optically by the formation of different ferroelastic domain patterns. This was ascribed to the growth of a low temperature monoclinic phase within the existing orthorhombic phase.

Detailed crystallographic studies have been undertaken recently. For a composition $K_{0.53}FeF_3$ a complex orthorhombic phase with $c \approx 2c_{TTB}$ was observed at room temperature using a combination of electron diffraction and single crystal X-ray diffraction [3]. This distortion was ascribed to a combination of charge-ordering (CO)

* Corresponding author. Present address: L. V. Kirensky Institute of Physics, Siberian Division, Russian Academy of Sciences, Akademgorodok, Krasnoyarsk 660036, Russia. Tel.: +7 391 249 45 07; fax: +7 391 2430 89 23.
E-mail address: flerov@iph.krasn.ru (I.N. Flerov).

http://dx.doi.org/10.1016/j.jfluchem.2014.09.031
0022-1139/

and ferroelectric (FE) symmetry-lowering, related to an octahedral-tilt mode.

A composition close to $K_{0.59}FeF_3$ was also studied [4], and found to exhibit the (CO) superstructure but not the octahedral tilt superstructure at room temperature. The (CO) superstructure gives rise to the $c = 2c_{TTB}$ cell axis, implying charge-ordering in alternating sites along the c-axis, in contrast to the early model [5]. The octahedral tilt (FE) super-structure was found below about 290 K. On heating, the orthorhombic—tetragonal transition for the basic subcell occurs above the previously reported ferroelectric transition at 570 K.

On the other hand, authors [9] have supposed that $K_{0.58}FeF_3$ compound consists of two phases: at 320 K *P4/mbm* (95%) and *Pbam* (5%); and at 270 K *Cmmm* (91%) and *Pbam* (9%). All phases are centrosymmetric and characterized by $c \approx c_{TTB}$.

The previous experimental studies suggest that there are several competing mechanisms of structural distortion inherent in this system. It is of particular interest to elucidate the nature and mechanism of the phenomena occurring in this type of materials. In this respect, we have carried out investigations of the structure, heat capacity, thermal expansion, and dielectric properties of KFe_2F_6 (alternatively formulated either $K_{0.5}FeF_3$ or $K_5Fe_{10}F_{30}$) ceramic samples over a wide temperature range (2–800 K).

Thermal properties are very sensitive to energy variations in the sample, regardless of their nature, and the relevant investigations can reliably reveal the associated phase transitions.

2. Experimental details

KFe_2F_6 was synthesized using solid state procedures. Starting fluorides KF, FeF_2 and FeF_3 were mixed in stoichiometric amounts and carefully ground and inserted in a Pt tube in glove box containing less than 3 ppm of H_2O and O_2. FeF_2 was prepared by fluorination of $FeCl_2$ under a stream of anhydrous HF at 400 °C for several hours, whereas FeF_3 was obtained by fluorination of $FeCl_3$ in pure F_2 atmosphere at 300 °C for several hours. KF was thoroughly dehydrated before use. Once sealed, the tube is heated following the cycle: 5 °C/min from 25 to 700 °C; 6 h at 700 °C, then cooled down 5 h to room temperature.

The powder diffraction data of KFe_2F_6 for Rietveld analysis were collected at $T = 133$ K, $T = 303$ K and $T = 453$ K with a Bruker D8 ADVANCE powder diffractometer (Cu$K\alpha$ radiation) with linear detector VANTEC. The beam was controlled by the 0.6 mm fixed divergence slit. An attachment Anton Paar TTK450 was used for all temperature measurements. The step size of 2θ was 0.016°, and the counting time was 2 s per step.

Mössbauer spectra were recorded on a MC114Em spectrometer with a $Co^{57}(Cr)$ source at the room temperature on powder samples of 10 mg/cm^2 thick.

The heat capacity of KFe_2F_6 was measured using two calorimetric methods. Low temperature measurements between 2 and 270 K were performed using a special option of a Physical Property Measurement System (Quantum Design, USA) by a relaxation technique on a sample with a mass of about 35 mg. Apiezon N grease was used to provide reliable thermal contact between the sample and the addenda. The absolute accuracy of the method was no worse than 1% over the entire temperature range.

In the middle temperature range (100–370 K), calorimetric studies were carried out by means of a homemade adiabatic calorimeter with three screens described in [10]. The sample with the mass of 35.24 mg was put into a heater consisting of an aluminum foil container with constantan wire cemented to its surface. A reliable thermal contact between the sample and the heater was provided by vacuum grease. Experimental measurements of heat capacity were performed using both the discrete ($\Delta T = 1.0$–2.5 K) and continuous [$dT/dt = (0.15$–$0.3)$ K/min] heatings. The error in heat capacity was about 0.2–0.4% in the whole temperature range investigated.

Thermal expansion was measured in the temperature range of 100–750 K with a heating rate of 1–3 K/min by means of a Netzsch model DIL-402C pushrod dilatometer. The ceramic samples were prepared in the form of a cylinder (8 mm in diameter and about 3 mm in length). The investigation was made under a helium atmosphere flowing at 40 mL/min.

The measurements of permittivity were carried out using an E7-20 immitance meter at a frequency of 1 kHz on heating and cooling at a rate of about 1.0 K/min in the temperature range 150–370 K. The study of dielectric properties was performed on the ceramic sample in the form of pressed pellet $5 \times 5 \times 1$ mm^3 with silver electrodes.

3. Results and discussion

3.1. Heat capacity

Calorimetric experiments identify two anomalies of heat capacity. The specific heat data as a function of temperature are plotted in Fig. 1. The $C_p(T)$ dependence demonstrates the classical picture of the λ-type transition around $T_m = 129.8 \pm 1$ K: with increasing temperature, the specific heat gradually rises on the low-temperature side of the transition and continuously decreases above T_m temperature, implying a substantial contribution of critical fluctuations, characteristic for magnetic phase transition (Fig. 1(a)). At $T_1 = 339.5 \pm 1$ K there is an additional anomaly typical of the phase transition. Moreover some peculiarity was observed in temperature range 250–280 K (at T_2).

The specific heat may involve several contributions $C_V = C_{lat} + C_{Sch} + \Delta C$. C_{lat} is associated with the lattice vibrations, C_{Sch} is the Schottky contribution, connected with potential splitting of magnetic levels of Fe ions in crystal field (Schottky anomaly) and ΔC is the anomalous contribution connected with phase transitions. The contributions of crystal defects and anharmonic effects are small and can be neglected. As a rule, the difference between C_V and C_p is important only at high temperatures. The lattice contribution to the specific heat C_{lat} can be approximated by combination of Debye and Einstein functions. The non-lattice contributions are described as the sum

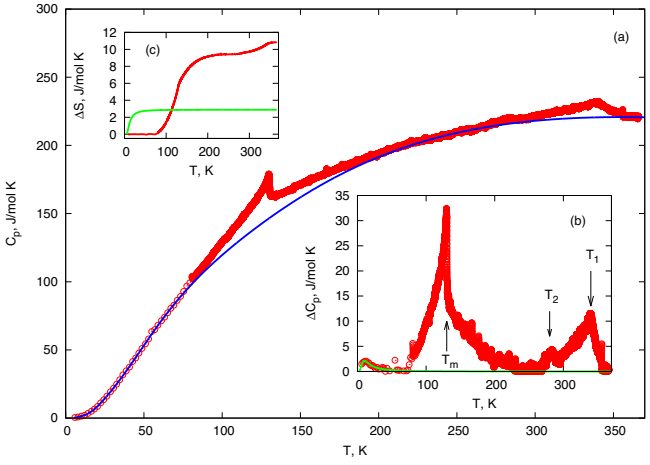

Fig. 1. Temperature dependences of heat capacity (a), anomalous contribution ΔC_p (b) and entropy change ΔS (c) for KFe_2F_6. (For interpretation of the references to color in this figure legend, the reader is referred to the web version of this article.)

$C_{non-lat} = C_{Sch} + \Delta C$. The Schottky contribution to the specific heat can be determined by the expression:

$$C_{Sch} = K_1 \left(\frac{K_2}{T}\right)^2 \frac{\exp(K_2/T)}{(1+\exp(K_2/T))^2}.$$

Varying the temperature intervals included in the fitting procedure, we have found that the average deviation of the experimental data from the smoothed curve does not exceed 1%. The anomalous part ΔC_p was found in a rather wide temperature ranges 60–230 K and 250–360 K (Fig. 1(b)). The relation between the maximum value of ΔC_p and C_{lat} does not exceed 17%. The solid (blue) line in Fig. 1(a) represents $C_{lat} + C_{Sch}$.

The total excess entropy associated with phase transitions was evaluated as $\Delta S = \int(\Delta C_p/T)dT = 11 \pm 1$ J/mol K and its temperature dependence is plotted in Fig. 1(c). The entropy change at magnetic phase transition is $\Delta S_m \approx 9.3$ J/mol K. The structural phase transition $G_0 - G_1$ at T_1 is characterized by small enough entropy $\Delta S_1 \approx 1.5$ J/mol K. Transformation $G_1 - G_2$ at T_2 is followed by very small change of structure that results in insignificant value of entropy $\Delta S_2 \sim 0.3$ J/mol K.

The Schottky-type anomaly with the maximum at ~11 K is associated with additional entropy ~3 J/mol K (solid green line in Fig. 1(c)) and, thus, full magnetic entropy is about ~13 J/mol K. But even this value is much less than maximum magnetic entropy $\Delta S = R\ln(6) + R\ln(5) = 28$ J/mol K for Fe^{2+} and Fe^{3+} ions which are in high-spin states (Fe^{3+}: $I = 5/2$, Fe^{2+}: $I = 2$) according to Mössbauer data [11].

To determine the lattice contribution C_{lat} we used quite rough approach describing it by combination of Debye and Einstein functions. Unfortunately, in low temperature region such a description of C_{lat} is as a rule invalid and correct extraction of heat capacity component connected with potential splitting of magnetic levels of Fe ions in crystal field (Schottky anomaly) is impossible. For more correct determination of a magnetic contribution to heat capacity, results of ab initio calculations of a phonon spectra or experimental data are necessary. Anyway the value of entropy change at magnetic phase transition much less than one, corresponding to full ordering of Fe nuclear spins.

3.2. Thermal expansion

Fig. 2(a) shows the temperature dependence of the coefficient of volume thermal expansion $\beta(T)$ in the temperature range of 100–550 K. The anomaly of β at magnetic phase transition was observed at $T_m = 133 \pm 3$ K and is very small, that may be connected with weak magnetoelastic interactions in this material (Fig. 2(b)). The anomalies associated with structural phase transitions take place at temperatures $T_2 \approx 248$ K and $T_1 = 342.5 \pm 3$ K which are in good agreement with the results of heat capacity measurements.

It was noted that at repeated measurements of thermal expansion after heating the sample to the temperatures $T > 600$ K, the anomaly at T_1 is shifted to lower temperatures and smeared (Fig. 2(c) curves 1, 2, 5, 6). Additional anomalous behavior was detected at high temperatures 600–700 K. Good repeatability of results in the temperature region 250–570 K was observed when the sample was heated only up to $T < 570$ K (Fig. 2(c) curves 3–4–5 and 7–8).

Comparing the dependencies of $C_p(T)$ and $\beta(T)$ near the phase transition temperature T_1 in the framework of the Pippard relation, one can obtain information about the susceptibility of a material to external pressure. The Pippard relation [12] connects the thermal expansion coefficient and the specific heat near the phase transition temperature by following way:

$$C_p = \frac{V_m T_1}{\gamma}\ \beta + \text{const}$$

where C_p—heat capacity, V_m—molar volume, T_1—phase transition temperature, $\gamma = dT_1/dp$.

Hereinafter the temperature dependence of heat capacity obtained by adiabatic calorimetry was used. Because the value of dT_1/dp strongly depends on the data closest to the critical temperatures, slight errors in the temperature scales of heat capacity measurements by adiabatic calorimeter (temperature sensor—platinum thermometer) and thermal expansion by dilatometer (temperature sensor—thermocouple) will produce significant errors in the results calculated from the Pippard theory. In this case the data on thermal expansion and heat capacity have been brought to one temperature scale by alignment of the phase transition temperatures.

The results of combined analysis of β and C_p below T_1 are shown in Fig. 3.

The experimental points fall approximately on straight lines and $dT_1/dp = 70 \pm 5$ K/GPa. That means the Pippard relation hold for phase transition in the temperature range about 5–40 K below the transition temperature T_1. Deviations from relation are observed in the vicinity of transition temperature, where the effects of the imperfections of the samples, dynamic nature of thermal expansion measurements and the difference of temperature scales for C_p and β measurements are the most significant.

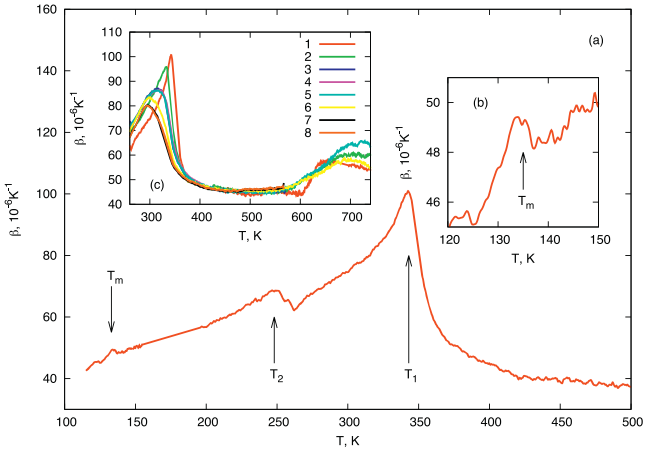

Fig. 2. Temperature dependencies of thermal expansion coefficient β for KFe_2F_6: (a)—at first measurement, (b)—near magnetic phase transition, (c)—at repeated measurements.

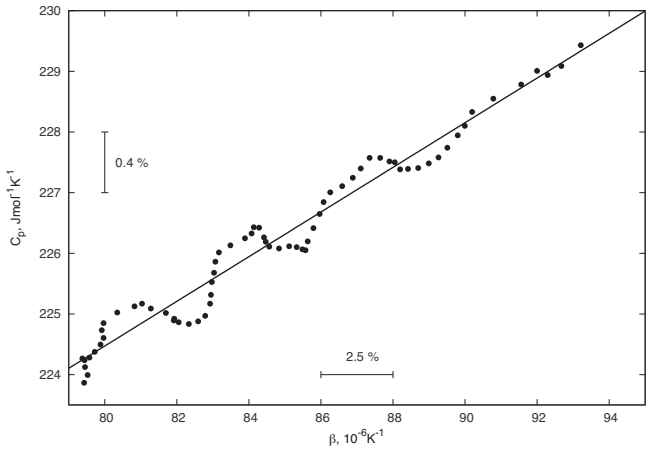

Fig. 3. Molar heat capacity C_p versus volume thermal expansion coefficient β for KFe_2F_6 below T_1.

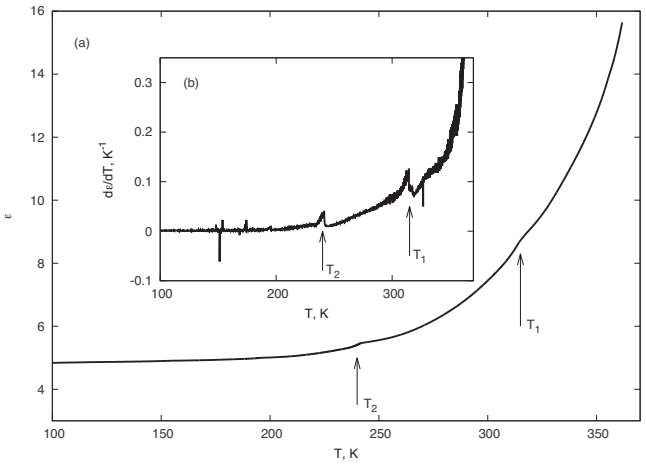

Fig. 4. Temperature dependencies of dielectric permittivity ε (a) and dε/dT derivative (b) of KFe_2F_6.

3.3. Dielectric permittivity

Fig. 4 shows small anomalies on the temperature dependence of the permittivity $\varepsilon(T)$. The more reliable evidence for the anomalous behavior one can obtain considering the dε/dT derivative (Fig. 4(b)).

Peculiar behavior was observed at temperatures $T_1 \approx 320$ K and $T_2 \approx 240$ K, which are in agreement with some phase transition temperatures found in experiments with adiabatic calorimeter and dilatometer. The behavior of the permittivity provides no evidence for the ferroelectric nature of transformations and polar phases in KFe_2F_6 in the temperature range studied. A rather strong $\varepsilon(T)$ increase above 270 K is, most likely, connected with dielectric losses in ceramic sample.

3.4. X-ray

Seventeen X-ray patterns were measured from 133 K to 453 K in a narrow 2θ range: 27.8–28.9° (step size 0.016°, 2 s per step), in order to evidence possible symmetry distortion at phase transitions (Fig. 5(a)). We have not found any peak splitting and superstructural reflections. Analysis of temperature dependence of Full Width at Half Maximum (FWHM) of two main reflections (4 0 0) and (4 1 0) allowed us to suggest that composition under study in this temperature range undergoes two structural phase transitions G_0 ($T_1 \approx 340$ K) → G_1 ($T_2 \approx 250$ K) → G_2 (Fig. 5(b) and (c)), that agrees well with the results of heat capacity and thermal expansion measurements.

In accordance with [9] high-temperature phase G_0 should be $P4/mbm$ and all diffraction lines of data obtained on KFe_2F_6 at $T = 453$ K are indexed by this cell. Because of this, crystal structure $P4/mbm$ was considered as starting model for Rietveld refinement using the program TOPAS 4.2 [13]. Refinement was stable and gives low R-factors (Table 1, Fig. 6). Crystal structure is shown in Fig. 7(a). Coordinates of atoms are presented in Table 2 and calculated chemical formula $K_{1.048}Fe_2F_6$ is close to suggested KFe_2F_6.

According to [4,5,9] the G_1 phase should be orthorhombic with space group either *Pba*2 or *Pbam*. Peak broadening (Fig. 5) agrees with these statements and two models of structure with two space groups above were used as starting models for Rietveld refinement. Low R-factors were found for both cases of refinements (Table 1, Fig. 8). Atomic coordinates are summarized in Table 2. One can see that models with both *Pba*2 and *Pbam* space groups are characterized by rather close R-factor values that prevents to choose the most convenient model. Structure of *Pbam* differs from *Pba*2 only by the presence of inversion center. Therefore, Fe and K ions can be displaced along c axis in *Pba*2 structure only. These differences affect the physical properties, partially on dielectric permittivity. As it was shown above, $\varepsilon(T)$ of KFe_2F_6 shows two very small anomalies at T_1 and T_2 which are not characteristic for ferroelectric phase transitions. Therefore we suppose that *Pbam* model is more probable one.

The possibility of the two phases coexistence below T_1, suggested in [9], was not considered because the refinement of X-ray pattern by single *Pbam* phase was successful. Large discrepancies on the difference Rietveld plot was not observed, and this is the reason why we should not take into account the second phase leading to unstable refinement. Actually, the resolution of X-ray diffractometer (XRD) is enough to discriminate the possibility of second phase existing. If two phases with similar cell parameters exist in sample then all of peaks should be broadened and can be detected by XRD. In our case only some of

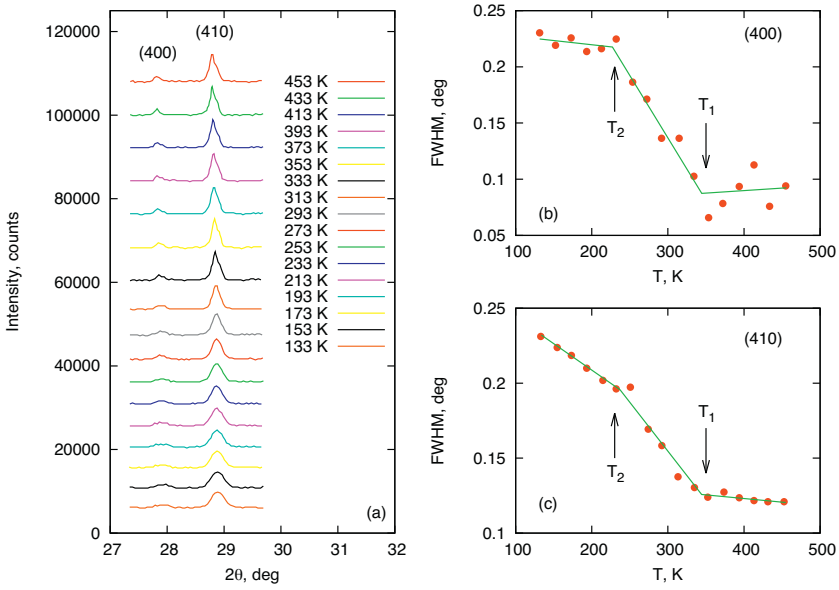

Fig. 5. Broadening of the main (4 0 0) and (4 1 0) reflections on cooling (a). Temperature dependencies of full width at half maximum (FWHM) for main reflexes (4 0 0) (b) and (4 1 0) (c). Arrows show temperature of possible phase transitions.

Table 1
Main parameters of processing and refinement of KFe_2F_6 at 453 K and 303 K.

Temperature	453 K	303 K	
Sp.Gr.	*P4/mbm*	*Pba2*	*Pbam*
a (Å)	12.6735 (3)	12.6600 (4)	12.6596 (5)
b (Å)	12.6735 (3)	12.6271 (5)	12.6273 (5)
c (Å)	3.96848 (8)	3.9529 (1)	3.9529 (1)
V (Å^3)	637.41 (3)	631.91 (4)	631.89 (4)
Z	5	5	5
2θ-interval (°)	5–120	5–120	5–120
Number of reflections	301	556	556
Number of parameters	52	67	55
R_{wp} (%)	1.40	1.67	1.68
R_p (%)	1.09	1.30	1.32
R_{exp} (%)	1.25	1.48	1.48
χ^2	1.11	1.13	1.14
R_B (%)	0.54	0.38	0.59

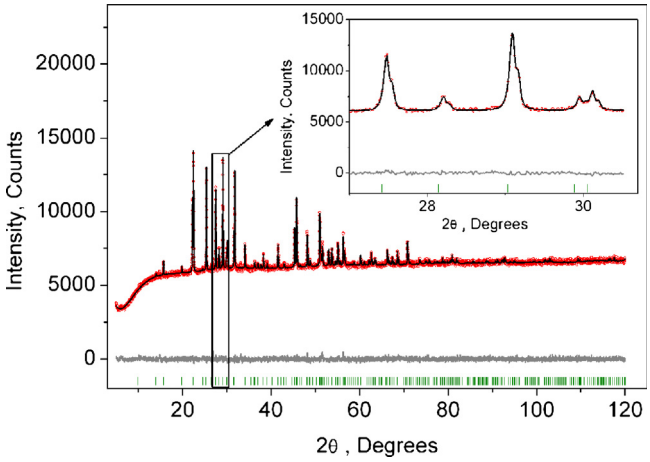

Fig. 6. The Rietveld difference plot of KFe_2F_6 at T = 453 K. Inset shows zoomed part of pattern with splitted peaks.

peaks are broadened due to phase transition (Figs. 6 and 8) and others remain unchanged. Such situation can be observed only in the case when the sample is almost single phase. In accordance with the resolution of XRD, only small amount (less than 5–7%) of other phase (*P4/mbm* or other then *Pbam*) can exist in the sample. In other case the difference Rietveld plot will be not so good as it was found by us.

Table 2
Fractional atomic coordinates and isotropic displacement parameters (Å^2).

	x	*y*	*z*	B_{iso}	Occ.
T = 453 K, *P4/mbm*					
Fe1	0.5	0	0.5	0.4 (2)	1
Fe2	0.2127 (3)	0.0752 (3)	0.5	0.40 (15)	1
K1	0.1715 (3)	0.3285 (3)	0	2.7 (2)	1
K2	0	0	0	0.5 (5)	0.622 (13)
F1	0.1447 (6)	−0.0705 (8)	0.5	1.50 (17)	1
F2	0.2799 (5)	0.2201 (5)	0.5	1.50 (17)	1
F3	0.3449 (8)	−0.0062 (4)	0.5	1.50 (17)	1
F4	0.5	0	0	1.50 (17)	1
F5	0.2071 (6)	0.0729 (7)	0	1.50 (17)	1
T = 303 K, *Pba2*					
Fe1	0	0.5	0.51 (3)	0.5 (3)	1
Fe2	0.0720 (7)	0.2117 (9)	0.52 (2)	0.5 (4)	1
Fe3	0.7872 (9)	0.0783 (8)	0.52 (2)	0.5 (3)	1
K1	0.1727 (11)	0.6715 (12)	0.04 (2)	1.9 (3)	1
K2	0	0	0	0.9 (8)	0.666 (20)
F1	0	0.5	0.01 (5)	1.0 (2)	1
F2	0.0917 (17)	0.205 (2)	0.04 (4)	1.0 (2)	1
F3	0.280 (2)	0.781 (2)	0.57 (2)	1.0 (2)	1
F4	0.7888 (19)	0.0515 (15)	0.00 (4)	1.0 (2)	1
F5	0.347 (2)	0.0087 (19)	0.58 (3)	1.0 (2)	1
F6	0.993 (2)	0.338 (2)	0.48 (3)	1.0 (2)	1
F7	0.142 (3)	0.070 (3)	0.47 (3)	1.0 (2)	1
F8	0.927 (3)	0.143 (3)	0.58 (3)	1.0 (2)	1
T = 303 K, *Pbam*					
Fe1	0	0.5	0.5	0.5 (2)	1
Fe2	0.0730 (8)	0.2113 (8)	0.5	0.5 (3)	1
Fe3	0.7881 (9)	0.0782 (8)	0.5	0.5 (3)	1
K1	0.1718 (11)	0.6711 (12)	0	1.3 (3)	1
K2	0	0	0	1.9 (7)	0.703 (19)
F1	0	0.5	0	1.6 (2)	1
F2	0.0924 (16)	0.203 (2)	0	1.6 (2)	1
F3	0.281 (2)	0.781 (2)	0.5	1.6 (2)	1
F4	0.7893 (19)	0.0519 (14)	0	1.6 (2)	1
F5	0.350 (2)	0.0087 (19)	0.5	1.6 (2)	1
F6	0.994 (2)	0.335 (2)	0.5	1.6 (2)	1
F7	0.142 (3)	0.068 (3)	0.5	1.6 (2)	1
F8	0.926 (3)	0.143 (3)	0.5	1.6 (2)	1

Fig. 5 shows that at T_2 the G_2 phase appears. This phase is characterized by deceleration of FHWM enlargement on cooling. It is very difficult to solve structure by using the X-ray data obtained. At least synchrotron data should be used to measure possible superstructural peaks and peak splitting. Now we can only state the fact of phase transition at T_2.

Crystal structure of *Pbam* is shown in Fig. 7(b) and one can see that some Fe ions can be ordered at phase transition *P4/*

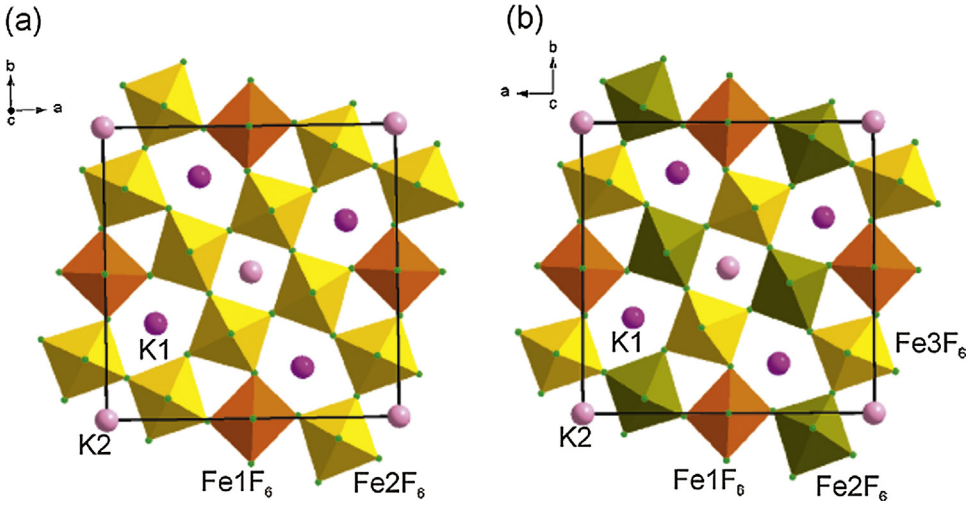

Fig. 7. Crystal structure of KFe_2F_6 at: (a) T = 453 K, *P4/mbm*; (b) T = 303 K, *Pbam*.

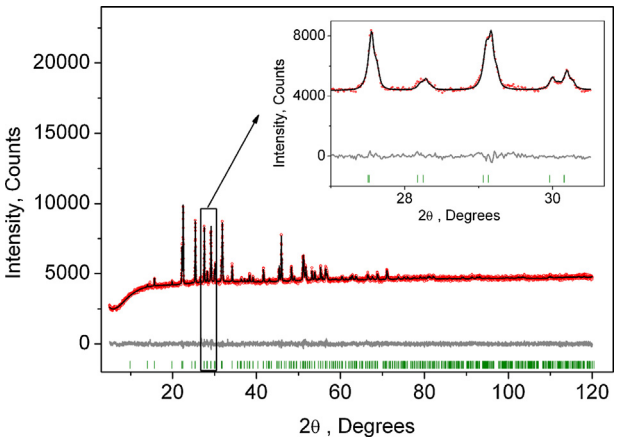

Fig. 8. The Rietveld difference plot of KFe_2F_6 at T = 303 K. Inset shows zoomed part of pattern with unsplitted peaks.

mbm → *Pbam*. There are two positions of Fe ions in G_0 phase: Fe1 and Fe2 (Fig. 7(a)). It is difficult to find Fe^{2+}/Fe^{3+} ratio in these sites from powder diffraction experiment, but we suggested that Fe^{2+} and Fe^{3+} ions are not ordered and distributed between these two sites. In the case of ordering, we could see their distinct positions using Fe–F distance because the average values of bond lengths d(Fe^{2+}–F) = 2.044 Å and d(Fe^{3+}–F) = 1.897 Å are quite different. However, structural refinement shows that Fe–F distances are averaged (Table 3) and thus there is no evidence of the Fe^{2+} and Fe^{3+} ions ordering. In $G_1 \equiv$ *Pbam* phase Fe2 site splits into two sites—Fe2 and Fe3. It's difficult to judge about Fe^{2+}/Fe^{3+} ordering using bond length because of big standard deviation (Table 3). However, these two sites should be characterized by different ratios Fe^{2+}/Fe^{3+} because the splitting of these sites has appeared, whereas in G_0 phase they were the same. Therefore we can only suggest that some process of Fe^{2+}/Fe^{3+} ordering happens during phase transition *P*4/*mbm* → *Pbam*.

3.5. Mössbauer spectra

Mössbauer spectra represent the sum of quadrupole doublets with different intensity and splitting (Fig. 9(a)). Identification of spectra is made in two steps. At the first step probability distribution of the quadrupole splitting is defined in experimental spectra. The sum of two groups of quadrupole doublets with a natural width is used. Amplitudes of doublets and two isomer chemical shifts corresponding to two groups of doublets were fitted. Probability distributions of quadrupole splitting for two valences, Fe^{3+} and Fe^{2+}, states of iron are shown in Fig. 9(b) and (c). Distribution P(QS) for a KFe_2F_6 shows two maxima for Fe^{3+} state and four maxima for Fe^{2+} state. These maxima testify to possible nonequivalent positions of iron.

At the second step, the model spectrum was formed on the base of information about the nonequivalent positions taken from P(QS). The model spectrum was fitted to an experimental spectrum at a variation of all hyperfine parameters. The result of fitting is presented in Table 4. Two positions are found for a Fe^{3+} state which differ by distortion size of local symmetry. Four nonequivalent positions are found for a Fe^{2+} state. These positions are caused by chaotic distribution of different valence cations on lattice sites. The asymmetrical electron shell of a Fe^{2+} cation is more sensitive to local symmetry causing identification of several nonequivalent positions. This situation may be connected with the "nonstoichiometry" of the sample under study as well as with possible phase separation/coexistence near room temperature leading to different local symmetry of Fe^{2+} ions.

The ratio between spectral areas belonging to Fe^{3+} and Fe^{2+} is about 45:55 and leads to the compound composition $K_{1.10}Fe^{2+}{}_{1.10}Fe^{3+}{}_{0.90}F_6$. This composition agrees within experimental errors with the results of X-ray study which gives the chemical formula $K_{1.048}Fe_2F_6$.

The results for sample after several (5) heating-cooling cycles (see Section 3.2) are presented in Fig. 9(d–f) and Table 5. In this case we observed the same ratio between spectral areas belonging to Fe^{3+} and Fe^{2+} and so the same chemical formula $K_{1.10}Fe_2F_6$. But the distributions of Fe^{3+} and Fe^{2+} ions between perovskite-like Fe2, Fe3 and extra-perovskite Fe1 positions are different (Table 5, Fig. 7). This result gives the key to interpretation of thermal expansion data for as-made and annealed (after heating up to 600–700 K) samples.

According to Mössbauer data the sample as prepared (with $T_1 > 300$ K) at room temperature represents, very likely, the mixture of two crystallographic modifications *P*4/*mbm* и *Pbam*. The annealed after several heating-cooling cycles sample, showing $T_1 < 300$ K, is in single tetragonal *P*4/*mbm* phase within an error of our measurements.

The irreproducibility of thermal expansion observed at the repeated heating can be connected with several reasons. First, with partial decomposition of the sample at the high temperatures that contradicts to the results of Mössbauer studies, where no change in composition was observed. The second reason may be, the most probable, is the change of cations ordering i.e. the change of Fe^{2+} and Fe^{3+} distribution in various (perovskite and extra-perovskite) octahedral positions as a result of sample cooling from high temperatures region.

In fact, a recent computational DFT study [14] suggests that there are a number of different charge-ordered models of similar

Table 3
The bond lengths of Fe–F of KFe_2F_6 in G_0 and G_1 phases.

G_0 phase			G_1 phase		
Bond	Distance (Å), multiplicity	Average bond length	Bond	Distance (Å), multiplicity	Average bond length
Fe1–F3	1.967 (6) × 4	1.97	Fe1–F5	1.90 (3) × 2	1.99
Fe1–F4	1.984 (5) × 2		Fe1–F1	1.976 (1) × 2	
			Fe1–F6	2.08 (3) × 2	
Fe2–F3	1.967 (9)	2.00	Fe2–F6	1.86 (3)	1.99
Fe2–F5	1.985 (1) × 2		Fe2–F2	1.995 (3) × 2	
Fe2–F1[i]	2.006 (9)		Fe2–F7	2.01 (3)	
Fe2–F2	2.024 (8)		Fe2–F3	2.04 (3)	
Fe2–F1	2.04 (1)		Fe2–F8	2.05 (3)	
			Fe3–F8	1.93 (3)	2.01
			Fe3–F3	1.99 (3)	
			Fe3–F4	2.004 (3) ×2	
			Fe3–F7	2.05 (4)	
			Fe3–F5	2.07 (2)	

[i] Symmetry operation: −*y*, *x*, *z*.

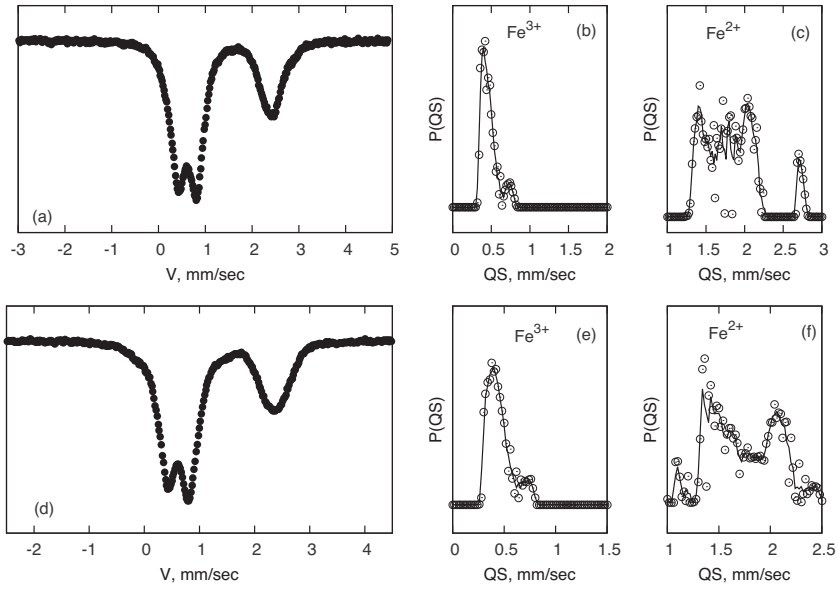

Fig. 9. Mössbauer spectra of KFe_2F_6 as-made sample (a) and sample after 5 heating-cooling cycles (d). Probability distribution of quadrupole splittings in experimental spectra for Fe^{3+} (b,e) and Fe^{2+} (c,f) cations.

energy, which can give drive distortions to ferroelectric states with differing polarization directions and magnitudes. Different charge-ordered structures were observed experimentally on the samples with closed concentration [4,9].

Mezzadri et al. [4] found that composition close to $K_{0.59}FeF_3$ corresponds to structural formula $K_4K_2[Fe^{2+}Fe^{3+}(Fe^{2+}{}_5Fe^{3+}{}_3)]F_{30}$, where Fe^{2+} and Fe^{3+} ions are ordered over perovskite and extra-perovskite positions, leading to $c = 2c_{TTB}$.

Reisinger et al. [9] supposed that structural formula of $K_{0.58}FeF_3$ compound at $T < 500$ K is approximately $K_4K_2[Fe^{3+}{}_2(Fe^{2+}{}_6Fe^{3+}{}_2)]F_{30}$, where Fe^{2+} and Fe^{3+} ions are disordered over perovskite positions and $c = c_{TTB}$. The as-made sample of $K_{0.58}FeF_3$, at ambient temperature, exists as a mixture of two distinct TTB phases *P*4/*mbm* and *Pbam*. On heating to 500 K, the phases merge to a single tetragonal phase. Subsequent in situ heating/cooling cycles were carried out on different samples in order to establish the reproducibility of the phase separation: heating the samples above 360 K (i.e., into the single tetragonal phase field) and then cooling at varying rates to 300 K shows that the ratio of the two phases coexisting below 340 K remains essentially unchanged.

Our initial sample corresponds approximately to the structural formula $K_4K[Fe^{2+}Fe^{3+}(Fe^{2+}{}_4Fe^{3+}{}_4)]F_{30}$ as long as the ratio of occupancies for two (perovskite and extra-perovskite) positions by Fe^{3+} ions is close enough to 1:4 (approximately 1.1:3.4).

Mössbauer spectra of the annealed (after several heating-cooling cycles) sample corresponds to the formula $K_4K[Fe^{2+}{}_2(Fe^{2+}{}_3Fe^{3+}{}_5)]F_{30}$. In this case the ratio of occupancies for two positions by Fe^{2+} ions is about 2:3. Fe^{3+} ions are located only in perovskite position.

Table 4
Mössbauer parameters of KFe_2F_6 (as-made sample). IS—isomer chemical shift relative to α-Fe, QS—quadrupole splitting, W—width of line, A—area of subspectrum (occupancy of an individual position).

IS (mm/s) (±0.005)	QS (mm/s) (±0.01)	W (mm/s) (±0.01)	A (±0.03)	Position
0.470	0.42	0.25	0.34	Fe^{3+}–1
0.467	0.72	0.24	0.11	Fe^{3+}–2
1.328	1.41	0.27	0.11	Fe^{2+}–1
1.366	1.67	0.27	0.16	Fe^{2+}–2
1.364	1.99	0.30	0.22	Fe^{2+}–3
1.304	2.67	0.34	0.06	Fe^{2+}–4

Table 5
Mössbauer parameters of KFe_2F_6 (sample after 10 heating-cooling cycles). IS—isomer chemical shift relative to α-Fe, QS—quadrupole splitting, W—width of line, A—area of subspectrum (occupancy of an individual position).

IS (mm/s) (±0.005)	QS (mm/s) (±0.01)	W (mm/s) (±0.01)	A (±0.03)	Position
0.46	0.34	0.33	0.45	Fe^{3+}
1.41	1.38	0.41	0.32	Fe^{2+}–1
1.27	2.17	0.39	0.23	Fe^{2+}–2

So, the distribution of Fe^{2+} and Fe^{3+} ions over perovskite and extra-perovskite positions may be changed after heating the sample up to 600–700 K and subsequent cooling, which may lead to a change of phase transition temperatures, diffused anomalies in thermal expansion and so on. Similar situation may be observed for samples prepared by different methods or at different conditions.

4. Concluding remarks

A detailed investigation of the thermodynamic properties and structure of the TTB fluoride KFe_2F_6 was performed in wide temperature region up to 800 K. The results obtained have allowed us to define at least two structural phase transitions between nonpolar phases $P4/mbm \rightarrow Pbam \rightarrow G_2$ at $T_1 \approx 340$ K and $T_2 \approx 250$ K without any doubling of unit cell parameters and one magnetic phase transition at $T_m \approx 133$ K.

Synthesis conditions and thermal prehistory of samples may change the distribution of Fe^{2+} and Fe^{3+} ions over crystal positions and lead to a change of distorted phases and phase transition temperatures. This may be the plausible reason why contradictory results were obtained for similar compounds. Further study is necessary to clarify this point. Synchrotron and Mössbauer investigations in wide temperature range would be very useful to elucidate the situation concerning possible phase coexistence and G_2 phase symmetry.

Acknowledgements

This work was supported by RFBR, project no. 12-02-00056, and the Council on Grants from the President of the Russian Federation

for the Support of Leading Scientific Schools of the Russian Federation (grant NSh-924.2014.2).

References

[1] A. Tressaud, R. de Pape, J. Portier, P. Hagenmuller, Bull. Soc. Chim. Fr. 10 (1970) 3411–3413.
[2] J. Ravez, S.C. Abrahams, R. de Pape, J. Appl. Phys. 65 (1989) 3987–3990.
[3] S. Fabbrici, E. Montanari, L. Righi, G. Calestani, A. Migliori, Chem. Mater. 16 (2004) 3007–3019.
[4] F. Mezzadri, S. Fabbrici, E. Montanari, L. Righi, G. Calestani, E. Gilioli, F. Bolzoni, A. Migliori, Phys. Rev. B: Condens. Matter 78 (2008) 064111.
[5] A.M. Hardy, G. Ferey, Acta Crystallogr., Sect. B: Struct. Sci. 29 (1973) 1654–1658.
[6] Y. Calage, S.C. Abrahams, J. Ravez, R. de Pape, J. Appl. Phys. 67 (1990) 430–433.
[7] J. Ravez, S.C. Abrahams, A.M. Mercier, L. Rabardel, R. de Pape, J. Appl. Phys. 67 (1990) 2681–2683.
[8] S. Ishihara, J.P. Rivera, E. Kita, Z.G. Ye, F. Kubel, H. Schmid, Ferroelectrics 162 (1994) 399–409.
[9] S.A. Reisinger, M. Leblanc, A.M. Mercier, C.C. Tang, J.R. Parker, F.D. Morrison, P. Lightfoot, Chem. Mater. 33 (2011) 5440–5445.
[10] A.V. Kartashev, I.N. Flerov, N.V. Volkov, R.A. Sablina, Phys. Solid State 50 (2008) 2115–2120.
[11] R. Blinc, G. Tavčar, B. Žemva, D. Hanžel, P. Cevc, G. Filipič, A. Levstik, Z. Jagličić, Z. Trontelj, N. Dalal, V. Ramachandran, S. Nellutla, J.F. Scott, J. Appl. Phys. 103 (2008) 074114.
[12] A.B. Pippard, The Elements of Classical Thermodynamics, Cambridge University Press, Cambridge, 1964.
[13] Bruker AXS, TOPAS V4: General Profile and Structure Analysis Software for Powder Diffraction Data.—User Manual, Bruker AXS, Karlsruhe, Germany, 2008.
[14] K. Yamauchi, S. Picozzi, Phys. Rev. Lett. 105 (2010) 107202.